

Méthodologies d'Estimation et de Détection Robuste en Conditions Non-Standards Pour le Traitement d'Antenne, l'Imagerie et le Radar

Jean-Philippe Ovarlez^{1,2}

¹SONDRA, CentraleSupélec, France

²French Aerospace Lab, ONERA DEMR/TSI, France

Joint works with F. Pascal, P. Forster, G. Ginolhac, M. Mahot, J. Frontera-Pons, A. Breloy,
G. Vasile, and many others

12^{ème} École d'Été de Peyresq
en Traitement du Signal et des Images
25 juin au 01 juillet 2017



Contents

- **Part A:**
Background on Radar, Array Processing, SAR and Hyperspectral Imaging
- **Part B:**
Robust Detection and Estimation Schemes
- **Part C:**
Applications and Results in Radar, STAP and Array Processing, SAR imaging, Hyperspectral Imaging

Part C

Applications and Results in Radar, STAP and
Array Processing, SAR imaging, Hyperspectral
Imaging

Part C: Contents

1 Applications and Results in Radar, STAP and Array Processing, SAR imaging, Hyperspectral Imaging

- Surveillance Radar
- STAP Applications
- SAR Imaging
- Hyperspectral Imaging

2 Conclusions and Perspectives

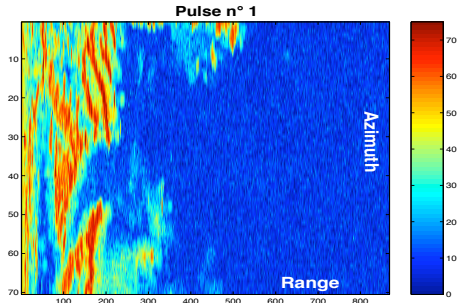
Outline

1 Applications and Results in Radar, STAP and Array Processing, SAR imaging, Hyperspectral Imaging

- Surveillance Radar
- STAP Applications
- SAR Imaging
- Hyperspectral Imaging

2 Conclusions and Perspectives

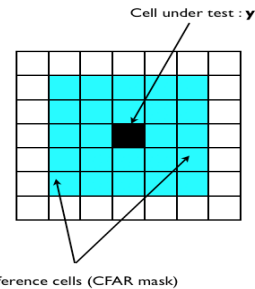
Data Description



- "Range-azimuth" map from ground clutter data collected by a radar from THALES Air Defense, placed 13 meters above ground and illuminating area at low grazing angle.
- Ground clutter complex echoes collected in 868 range bins for 70 different azimuth angles and for $m = 8$ pulses.

Data processing

- Rectangular CFAR mask 5×5 for $0 \leq k \leq m$ different steering vectors \mathbf{p}_k .



$$\mathbf{p}_k = \begin{pmatrix} 1 \\ \exp\left(\frac{2i\pi(k-1)}{m}\right) \\ \exp\left(\frac{2i\pi(k-1)2}{m}\right) \\ \vdots \\ \exp\left(\frac{2i\pi(k-1)(m-1)}{m}\right) \end{pmatrix}$$

- For each y , computation of associated detectors $\Lambda_{ANMF}(\widehat{\Sigma}_{Tyler})$ and $\Lambda_{ANMF}(\widehat{\Sigma}_{NSCM})$
- Mask moving all over the map.

False Alarm Regulation Results on Experimental Data (Surveillance Radar)

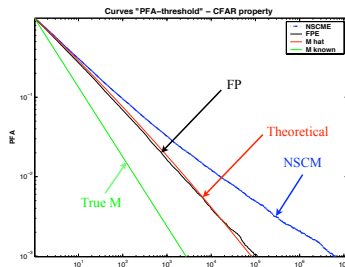
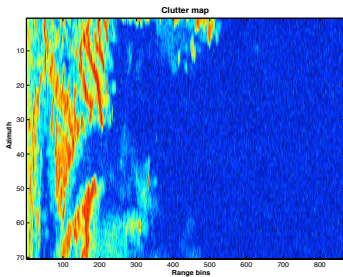
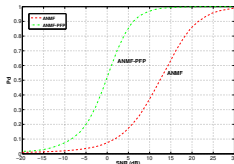
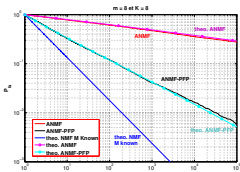


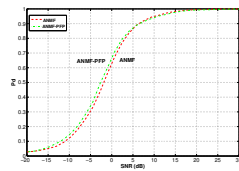
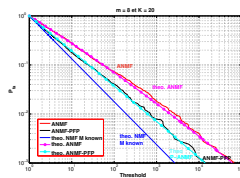
Figure: ANMF with Tyler's M-estimate - False alarm regulation for $\mathbf{p}_0 = (1 \dots 1)^T$.

Black curve fits red curve until $PFA = 10^{-3}$ [Ovarlez et al.] in [Greco and Maio, 2016].

False Alarm Regulation Results on Experimental Data (Surveillance Radar) [Pailloux et al., 2011, Pailloux, 2010]



Persymmetric Tyler-ANMF and Tyler ANMF on THALES dataset - $m = 8, n = 8$



Persymmetric Tyler-ANMF and Tyler ANMF on THALES dataset - $m = 8, n = 20$

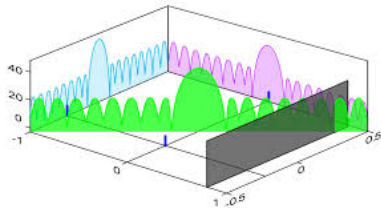
Outline

1 Applications and Results in Radar, STAP and Array Processing, SAR imaging, Hyperspectral Imaging

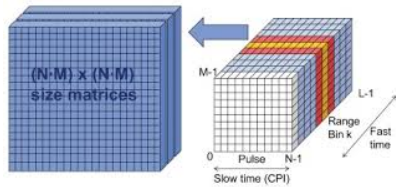
- Surveillance Radar
- **STAP Applications**
- SAR Imaging
- Hyperspectral Imaging

2 Conclusions and Perspectives

Space Time Adaptive Processing: Principles



(a) STAP principles



(b) STAP datacube

$$\mathbf{p}(\theta, f_d) = \begin{pmatrix} 1 \\ \exp(-2i\pi d \sin(\theta)/\lambda) \\ \vdots \\ \exp(-2i\pi(N-1)d \sin(\theta)/\lambda) \end{pmatrix} \otimes \begin{pmatrix} 1 \\ \exp(-2i\pi f_d T_r) \\ \vdots \\ \exp(-2i\pi f_d(M-1)T_r) \end{pmatrix}$$

STAP Principles [Ovarlez et al., 2011b]

Problem: Using joint spatial and time measurements, estimate the position (angle) and the Doppler frequency (speed) of the target
⇒ use of the ANMF with a particular steering vector

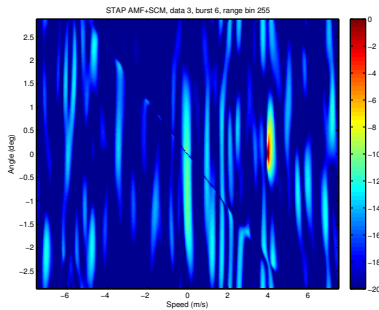
Data parameters: real clutter with synthetic target

X-Band $\simeq 10^9$ Hz, wavelength $\lambda = 0.03\text{m}$, flight speed $v = 100\text{m/s}$, distance to the scene 30km, 5 deg of incidence, PRF (Pulse Repetition Frequency) of 1 kHz, inter-sensor distance $d = 0.3\text{m}$, 12 trials with $n = 410$ range bins, $M = 64$ pulses and $N = 4$ sensors.

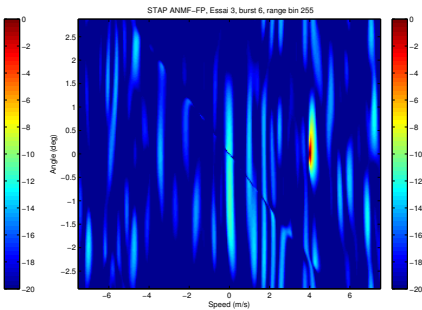
This means observations of size $m = 256$ while $n \leq 410$!

Clutter more or less homogeneous **BUT** some targets (outliers) could be present in the secondary data

No target is present in the secondary data - homogeneous noise



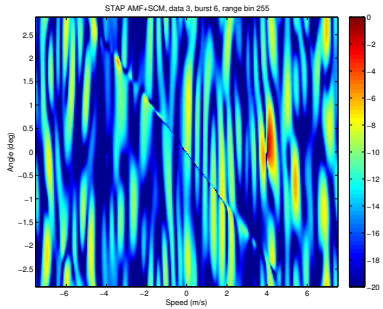
(c) AMF detector with the SCM



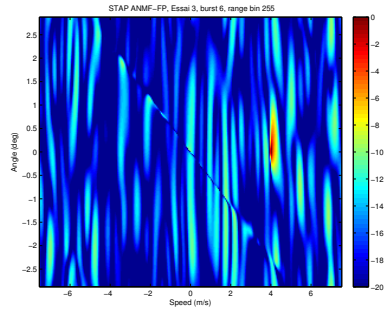
(d) ANMF detector with Tyler's est.

Figure: Doppler-angle map for the range bin 255 with $n = 404$ secondary data (targets and guard cells are removed) and $m = 256$

Two targets (4m/s and -4m/s) are present in the secondary data - homogeneous noise



(a) AMF detector with the SCM



(b) ANMF detector with Tyler's est.

Figure: Doppler-angle map for the range bin 255 with $n = 404$ secondary data (guard cells are removed) and $m = 256$

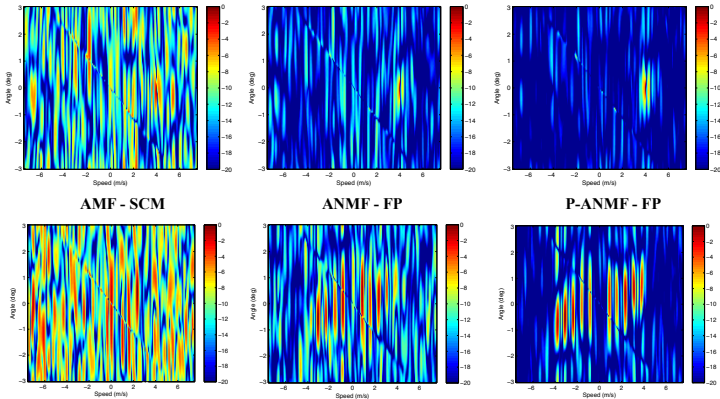


Figure: Doppler-angle map for the range bin 255 with $n = 404$ secondary data (guard cells are removed) and $m = 256$

Extended Low Rank Detectors

[Ginolhac et al., 2012, Ginolhac et al., 2013]

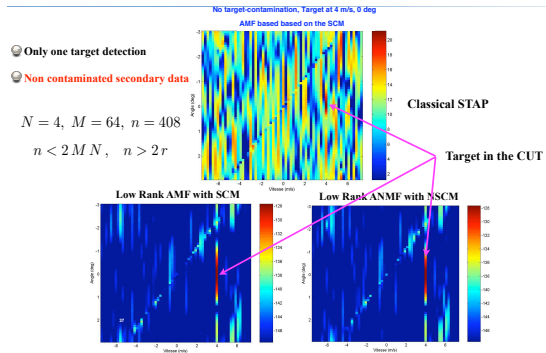


Figure: Doppler-angle map for the range bin 255 with $n = 100 < m$ secondary data (guard cells are removed) and $m = 256$

Extended Low Rank Detectors [Ginolhac et al., 2011]

Only one target (4m/s) in the CUT

Contaminated secondary data
(two targets at 4m/s and -4m/s)

$$N = 4, M = 64, n = 410$$

$$n < 2MN, \quad n > 2r$$

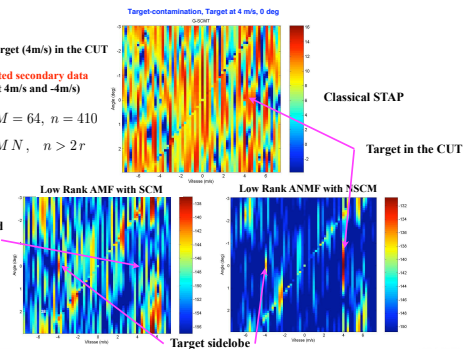
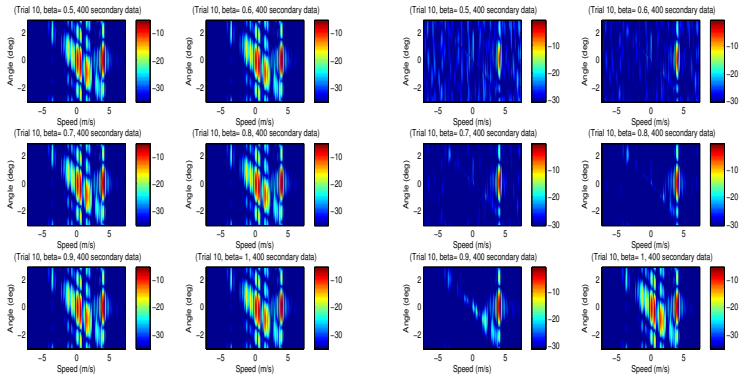


Figure: Doppler-angle map for the range bin 255 with $n = 100 < m$ secondary data (guard cells are removed) and $m = 256$

Application of Shrinkage to STAP [Pascal et al., 2014]

Applications to STAP data for \neq values of β , $m = 256$ and $n = 400$

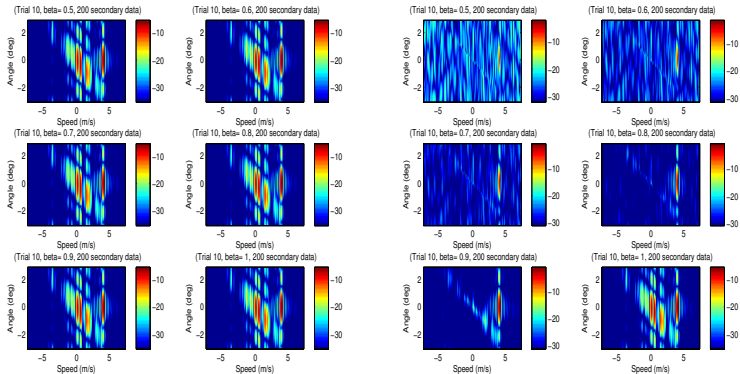


(a) SCM

(b) Shrinkage FPE

Application of Shrinkage to STAP [Pascal et al., 2014]

Applications to STAP data for \neq values of β , $m = 256$ and $n = 200 \leq m$



(c) SCM

(d) Shrinkage FPE

Outline

1 Applications and Results in Radar, STAP and Array Processing, SAR imaging, Hyperspectral Imaging

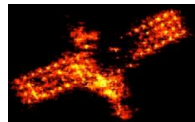
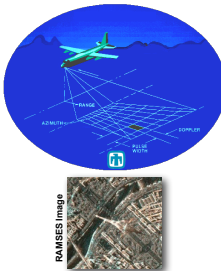
- Surveillance Radar
- STAP Applications
- SAR Imaging**
- Hyperspectral Imaging

2 Conclusions and Perspectives

Background on SAR and Radar Imaging



ONERA RAMSES Image



ONERA ISAR Image



ONERA RAMSES Image

Radar Imaging allows to build more and more precise images:

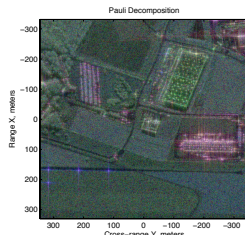
- Current use of **very high spectral bandwidth** and **very high angular bandwidth** leading to very high spatial resolution,
- Application to monitoring (detection, change detection), classification, 3D reconstruction, EM analysis, etc.

These applications require some physical diversity to reach good performances.

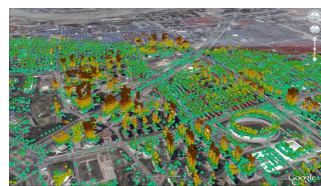
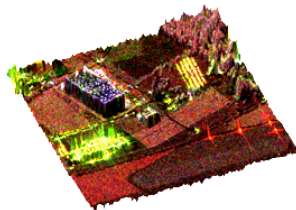
Multi-Channel SAR Images

Multi-channel SAR images automatically propose this diversity through:

- polarimetric channels (POLsar), interferometric channels (INSAR), polarimetric and interferometric channels (POLINSAR),
- multi-temporal, multi-passes SAR Image, etc.



EM behavior of the terrain
in POLsar images

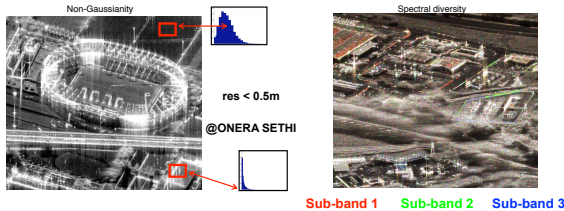


Almost all the conventional techniques of detection, parameters estimation, speckle filtering techniques, classification in multi-channel SAR images (e.g. polarimetric covariance matrix, interferometric coherency matrix) are based on the **multivariate statistic**.

Mono-Channel SAR Images

For mono-channel SAR Images, each pixel of the spatial image is **only** characterized by a complex amplitude and we don't have directly access to this diversity. Moreover,

- very high resolution SAR images are more and more complex, detailed, heterogeneous,
- the spatial statistic of SAR images may be **not at all Gaussian** !
- SAR pixels may be **dispersive** (or colored) and **anisotropic**.



Challenging Problems

- How to retrieve, how to exploit this diversity (dispersive and anisotropic information) from mono-channel SAR image ?
- How to derive Multivariate Adaptive Detectors on a mono-channel complex SAR image ?

Conventional Principle of Radar/SAR Imaging

Conventional Fourier Imaging (laboratory, SAR, ISAR):

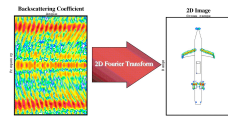
- Assumptions of white and isotropic bright points
- It does not exploit the potential non-stationarities or diversities of the scatterers
- Hypothesis of bright points modeling: all the scatterers localized in x and characterized by the complex spatial amplitude distribution $I(x)$ have **the same behavior** for any wave vector $\mathbf{k} = \frac{2f}{c}(\cos\theta, \sin\theta)^T$. After some processing, the backscattering coefficient $H(\mathbf{k})$ acquired by the radar is simply related to the SAR image $I(x)$ through:

$$H(\mathbf{k}) = \int_{\mathcal{D}_x} I(x) \exp(-2i\pi\mathbf{k}^T x) dx$$

- The SAR image $I(x)$ is then obtained through the Inverse Fourier Transform:

$$I(x) = \int_{\mathcal{D}_k} H(\mathbf{k}) \exp(2i\pi\mathbf{k}^T x) dk$$

With this model, all information relative to frequency f and angle θ are lost. Hence, spectral and angular diversities are lost.



Time-Frequency Distributions for SAR Imaging - Key Idea

Time-Frequency Distributions are generally devoted to non-stationary time signals analysis (e.g. spectral components varying with time). They can be easily extended in 2D.

Key idea: In the context of SAR Imaging, Time-Frequency Analysis allows:

- to highlight the coloration and anisotropy properties of monodimensional SAR scatterers,
- to characterize each pixel of the complex SAR image with a vector of information related to angular or/and frequency behaviors.

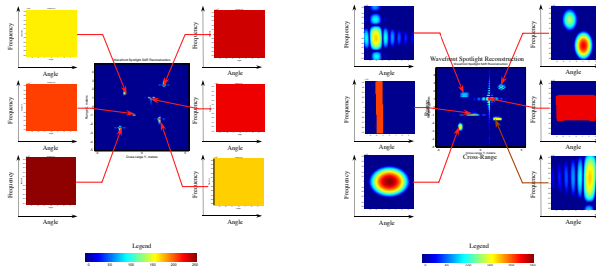
LTFD analysis and the physical group theory (Heisenberg or affine group) allow to construct **hyperimages** [Bertrand et al., 1991, Bertrand et al., 1994, Bertrand and Bertrand, 1996] through:

$$\tilde{I}(\mathbf{r}_0, \mathbf{k}_0) = \langle H(\cdot), \Psi_{\mathbf{r}_0, \mathbf{k}_0}(\cdot) \rangle = \int_{\mathcal{D}_{\mathbf{k}}} H(\mathbf{k}) \Psi_{\mathbf{r}_0, \mathbf{k}_0}^*(\mathbf{k}) d\mathbf{k},$$

where $\Psi_{\mathbf{r}_0, \mathbf{k}_0}(\mathbf{k})$ is a family of wavelet bases (Gabor, wavelet) generated from a mother wavelet $\phi(f, \theta)$ through the chosen physical group of transformation (translations, scale in frequency, etc.) and where $\mathcal{D}_{\mathbf{k}}$ is the spectral/angular support of the wavelet Ψ .

Highlighting the Spectral and Angular Behaviors of Scatterers

Some examples of synthetic hyperimages $\tilde{I}(\mathbf{r}_0, \mathbf{k}_0)$:



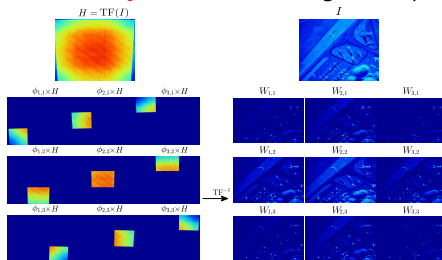
Isotropic and white scatterers.

Anisotropic and colored scatterers.

- An isotropic and white scatterer is mainly located on a pixel of SAR image,
- An anisotropic and colored scatterer may naturally spread out in spatial domain !

From Mono-Channel to Multi-Channel SAR Image

Example of $N_f = 3$ sub-bands and $N_\theta = 3$ sub-looks image decomposition:



Exploitation of the diversity

Each pixel i of the mono-channel SAR image can now be characterized by a N -vector $\mathbf{x}_i = [W_{1,1}^i, \dots, W_{N_f N_\theta}^i]^T$ of information ($N = N_f N_\theta$) related to **dispersion** in frequency domain and **anisotropy** in angular domain. Which multivariate statistic can characterize the vector \mathbf{x}_i ?

Robust Detection Schemes for CES distributions

In CES distributed noise, a well known two-step detector with nice properties have been derived [Conte et al., 1995, Kraut and Scharf, 1999]:

ANMF test:

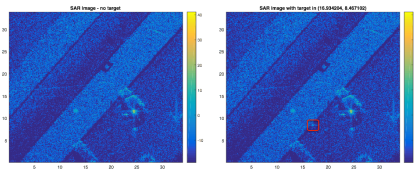
$$\Lambda_{ANMF}(\mathbf{x}) = \frac{\left| \mathbf{p}^H \hat{\Sigma}_{TE}^{-1} \mathbf{x} \right|^2}{\left| \mathbf{x}^H \hat{\Sigma}_{TE}^{-1} \mathbf{x} \right| \left| \mathbf{p}^H \hat{\Sigma}_{TE}^{-1} \mathbf{p} \right|} \stackrel{H_1}{\underset{H_0}{\gtrless}} \lambda_{ANMF},$$

where $\hat{\Sigma}_{TE}$ stands for Tyler's estimator.

- The ANMF is **scale-invariant** (homogeneous of degree 0), i.e.
 $\forall \alpha, \beta \in \mathbb{R}, \Lambda_{ANMF}(\alpha \mathbf{x}, \beta \hat{\Sigma}_{TE}) = \Lambda_{ANMF}(\mathbf{x}, \hat{\Sigma}_{TE}),$
- It is CFAR w.r.t the covariance/scatter matrix, CFAR w.r.t the texture,
- Under H_0 hypothesis, P_{fa} and λ_{ANMF} are related to a theoretical closed-form expression [Pascal, 2006, Pascal et al., 2006, Pascal et al., 2008]. This allows to set up a fixed detection threshold λ_{ANMF} anywhere in the heterogeneous and non-Gaussian SAR image.

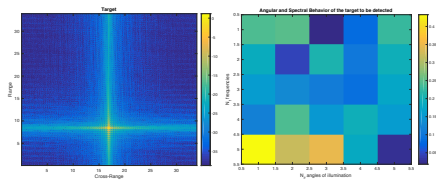
Results - SANDIA Dataset

Dataset from SANDIA National Laboratories



Left: Original SAR Image without target.
Right: SAR image with specific embedded target.

Artificial embedded target



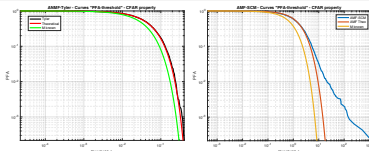
Left: SAR Image of the target. Right: True target response p in angular and spectral spaces ($N_\theta = 5$ sub-looks, $N_f = 5$ sub-bands).

Analysis of Performance

- Evaluation the CFAR property of the AMF and ANMF detectors,
- Comparison of the target detection performance between AMF and ANMF.

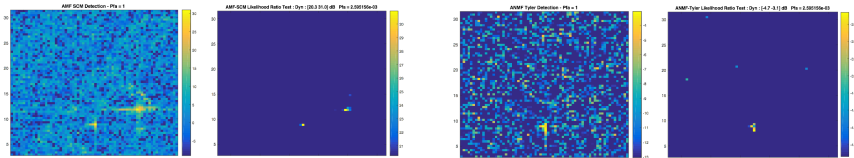
Analysis of performance

Perfect PFA regulation with ANMF-TE but poor PFA regulation for AMF-SCM



Left: FA Regulation with ANMF-Tyler. Right: FA Regulation with AMF-SCM. $N_\theta = 5$, $N_f = 5$, $K = 88$.

Better target detection for ANMF-TE [Ovarlez et al., 2017, Mian et al., 2017]



Left: Full AMF-SCM detection test, $P_{fa} = 1$. Right:

Jean-Philippe Ovarlez

Left: ANMF-TE detection test, $P_{fa} = 1$. Right:

12ème École d'Été de Peyresq

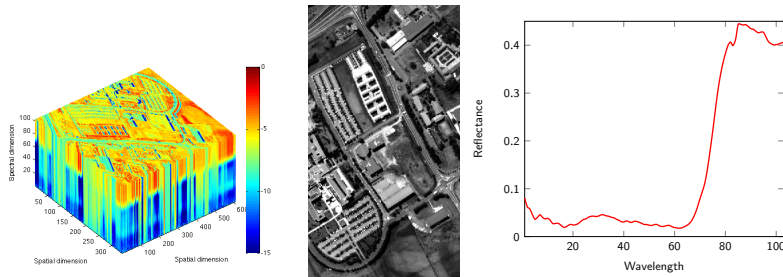
Outline

1 Applications and Results in Radar, STAP and Array Processing, SAR imaging, Hyperspectral Imaging

- Surveillance Radar
- STAP Applications
- SAR Imaging
- Hyperspectral Imaging

2 Conclusions and Perspectives

Hyperspectral Imaging (HSI)



- **Anomaly Detection**

To detect all that is "different" from the background (Mahalanobis distance) - No information about the targets of interest available [Frontera-Pons et al., 2016].

- **"Pure" Detection**

To detect targets characterized by a given spectral signature \mathbf{p} - Regulation of False Alarm [Ovarlez et al., 2011a, Frontera-Pons et al., 2017].

The hyperspectral data are **real** and **positive** as they represent radiance or reflectance.

- A mean vector has been included in the model and estimated jointly with the scatter matrix,
- The real data has been transformed into complex ones by a linear Hilbert filter and then be decimated by a factor 2 (principle of analytic signals)



Original data set (Hymap data)

Problem

Now, the statistical mean is non null \Rightarrow M-estimator of the mean is required

$$\hat{\mu} = \frac{\sum_{i=1}^n u_1(t_i) \mathbf{z}_i}{\sum_{i=1}^n u_1(t_i)} \text{ and } \hat{\Sigma} = \frac{1}{n} \sum_{i=1}^n u_2(t_i^2) (\mathbf{z}_i - \hat{\mu})(\mathbf{z}_i - \hat{\mu})^H,$$

where $t_i = ((\mathbf{z}_i - \hat{\mu})^H \hat{\Sigma}^{-1} (\mathbf{z}_i - \hat{\mu}))^{1/2}$ and $u_1(\cdot), u_2(\cdot)$ denote any real-valued *weight functions* (following the conditions of Maronna).

⚠ No proofs of existence, uniqueness, consistency and convergence of the recursive algorithm!

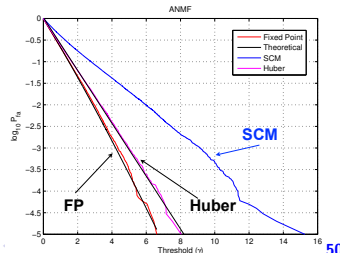
ANMF and M-estimates for Hyperspectral target detection [Frontera-Pons et al., 2014, Frontera-Pons et al., 2017]

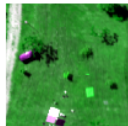
$$\Lambda(\mathbf{c}) = \frac{\left| \mathbf{p}^H \widehat{\Sigma}^{-1} (\mathbf{c} - \widehat{\mu}) \right|^2}{(\mathbf{p}^H \widehat{\Sigma}^{-1} \mathbf{p}) \left((\mathbf{c} - \widehat{\mu})^H \widehat{\Sigma}^{-1} (\mathbf{c} - \widehat{\mu}) \right)} \stackrel{H_1}{\gtrless} \stackrel{H_0}{\gtrless} \lambda$$

$$P_{fa} = (1 - \lambda)^{\frac{n-1}{\sigma_1} - m + 1} {}_2F_1 \left(\frac{n-1}{\sigma_1} - m + 2, \frac{n-1}{\sigma_1} - m + 1; \frac{n-1}{\sigma_1} - 1; \lambda \right),$$

where the parameter σ_1 is very close to 1 but depends on the M-estimator:
for Tyler's estimate, $\sigma_1 = (m+1)/m$.

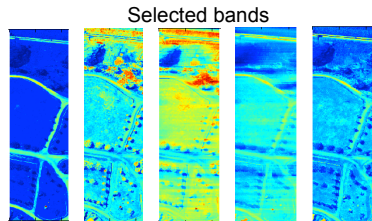
- This two-step GLRT test is homogeneous of degree 0: it is independent of any particular Elliptical distribution: CFAR texture and CFAR Matrix properties,
- Under homogeneous Gaussian region, it reaches the same performance than those of the detector built with the SCM estimate.



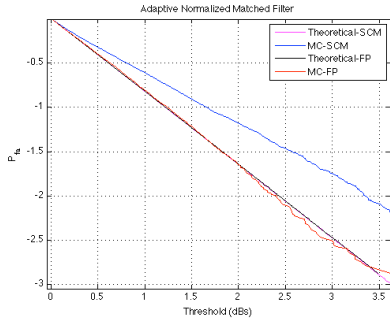


Extracted region :

- ▶ 100 x 100 pixels,
- ▶ 5 bands,
- ▶ Sliding Window: 19x19

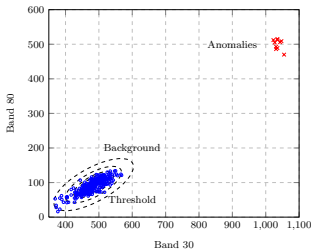


Original data set



GLRT RX Anomaly Detector: Mahalanobis Distance [Reed and Yu, 1990]

Binary Hypotheses test: $\begin{cases} H_0 : \mathbf{c} = \mathbf{b} & \mathbf{c}_1, \dots, \mathbf{c}_n \\ H_1 : \mathbf{c} = A\mathbf{p} + \mathbf{b} & \mathbf{c}_1, \dots, \mathbf{c}_n \end{cases}$ where $\mathbf{b} \sim \mathcal{CN}(\mathbf{0}, \mathbf{M})$ and $\mathbf{c}_i \sim \mathcal{CN}(\mathbf{0}, \mathbf{M})$, A known and \mathbf{p} unknown



$$\text{denoting } \hat{\mu} = \frac{1}{n} \sum_{i=1}^n c_i$$

$$RXD_{SCM}(\mathbf{c}) = (\mathbf{c} - \hat{\mu})^H \hat{\mathbf{S}}_n^{-1} (\mathbf{c} - \hat{\mu}) \stackrel{H_1}{\gtrless} \stackrel{H_0}{\lessgtr} \lambda$$

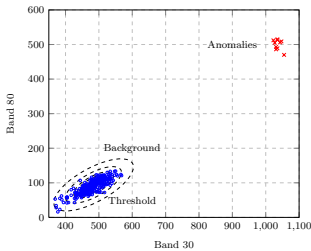
(Hotelling T^2 distributed)

$$\frac{n-m}{m(n+1)} RXD_{SCM}(\mathbf{c}) \sim F_{m,n-m}$$

- Derived and valid only under Gaussian hypotheses,
- Its false alarm rate is independent of the covariance matrix: CFAR-matrix property in homogeneous Gaussian data.

Extended GLRT RX Anomaly Detector: Mahalanobis Distance [Frontera-Pons et al., 2014, Frontera-Pons et al., 2017]

Binary Hypotheses test: $\begin{cases} H_0 : \mathbf{c} = \mathbf{b} \\ H_1 : \mathbf{c} = A\mathbf{p} + \mathbf{b} \end{cases}$ $\mathbf{c}_1, \dots, \mathbf{c}_n$ where $\mathbf{b} \sim CE(\boldsymbol{\mu}, \boldsymbol{\Sigma}, g_z)$
and $\mathbf{c}_i \sim CE(\boldsymbol{\mu}, \boldsymbol{\Sigma}, g_z)$, A known and \mathbf{p} unknown

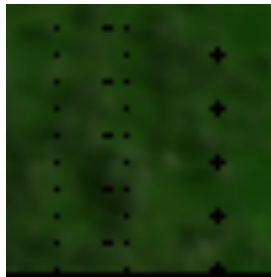


$$RXD_{M-est}(\mathbf{c}) = (\mathbf{c} - \hat{\boldsymbol{\mu}})^H \hat{\boldsymbol{\Sigma}}^{-1} (\mathbf{c} - \hat{\boldsymbol{\mu}}) \stackrel{H_1}{\gtrless} \lambda \stackrel{H_0}{\lessgtr} \lambda$$

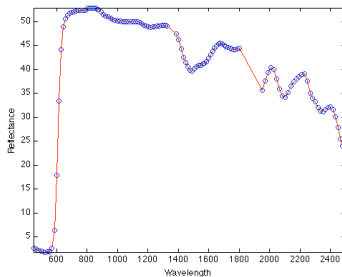
where $\hat{\boldsymbol{\Sigma}}$ and $\hat{\boldsymbol{\mu}}$ are M-estimates
of the location and scale

- Derived and valid for any Elliptical Contoured Distributions,
- Its false alarm rate unfortunately depends on texture statistic of the data.

Anomaly Detection Results on Artificial Targets



Original image (Forest Region)

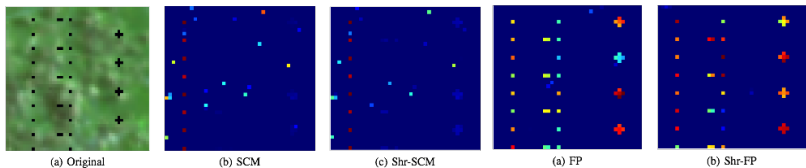


Target Spectrum

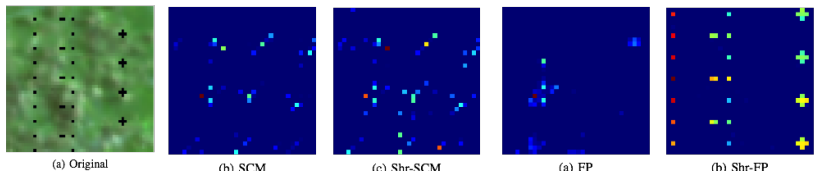
50 x 50 pixels, 126 spectral bands



Anomaly Detection Results on Artificial Targets



Extended Kelly AD built with conventional and robust estimates for artificial targets in real HSI with all the bands ($m = 9$, $n = 80$, same PFA = 0.03).

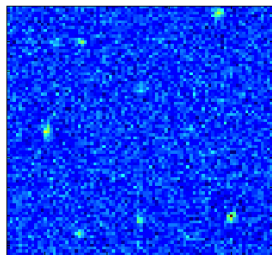


Extended Kelly AD built with conventional and robust estimates for artificial targets in real HSI with all the bands ($m = 126$, $n = 288$, same PFA = 0.03)

Galaxies Anomaly Detection Results on MUSE data

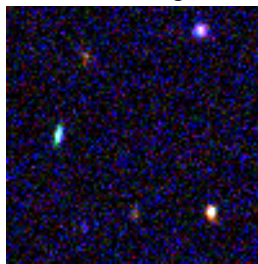
Problem of detecting galaxies in HS MUSE (Multi Unit Spectroscopic Explorer) data (465- 930 nm)

Classical RXD



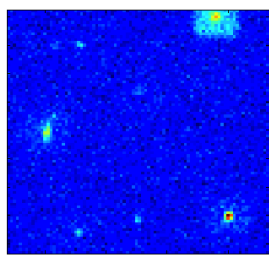
$RXD_{SCM}(\mathbf{c})$

Muse Image



300 x 300 pixels
3578 spectral bands

Extended RXD



$RXD_{FP}(\mathbf{c})$

Outline

- 1 Applications and Results in Radar, STAP and Array Processing, SAR imaging, Hyperspectral Imaging**
 - Surveillance Radar
 - STAP Applications
 - SAR Imaging
 - Hyperspectral Imaging
- 2 Conclusions and Perspectives**

Conclusions

When the background is non-Gaussian and/or heterogeneous, the conventional detectors (AMF or sub-optimal CFAR tests) are not at all optimal and lead to poor false alarm regulation and poor detection performance,

The SIRV and CES background modeling allows to take into account the background complexity: the non-Gaussianity, the temporal background fluctuations and the spatial background power fluctuations,

Using this model, the ANMF detector built with the Fixed Point (or other MI-estimators) background covariance matrix estimator is shown to be CFAR-texture, CFAR-matrix and exhibits nice properties (robustness) and very good detection performance,

Conclusions

Taking into account additional *a priori* properties on the covariance matrix structure (low rank, persymmetry, Toeplitz, ...) can lead to a appreciable gain for small numbers of secondary data,

These methods have been applied for many problems involving covariance matrix estimation: STAP detection, SAR detection (FOPEN), Polarimetric/Interferometric SAR detection and classification, SAR and Hyperspectral Change Detection, SAR and Hyperspectral time-series analysis, Hyperspectral Anomaly detection, Hyperspectral detection.

On-going works and Perspectives

Link with **Random Matrix Theory**: for high dimensionality data (ex: hyperspectral, STAP), strong statistical connection with Robust Estimation theory: see current works of R. Couillet, and F. Pascal,

Robust estimation of structured covariance matrices [Y. Sun, D. P. Palomar, A. Breloy, G. Ginolhac, F. Pascal, P. Forster],

Joint location and scale with M-Estimators (non-centered multivariate data, e.g. hyperspectral data) [J. Frontera, F. Pascal, J.P. Ovarlez],

How to deal with non i.i.d secondary data? RMT approach: [R. Couillet, F. Pascal, J.P. Ovarlez], VARMA approach: [W. Ben-Abdallah, P. Bondon, J.P. Ovarlez],

On-going works and Perspectives

No secondary data: [C. Ren, N. El-Korso, P. Forster, A. Breloy, J.P. Ovarlez],

M-Estimators and Riemannian Geometry: [F. Barbaresco], [F. Pascal, G. Ginolhac, A. Renaux],

Shrinkage of M-Estimators: [A. Wiesel, Y. Abramovitch, O. Besson, F. Pascal, E. Ollila, ...], [Q. Hoarau, G. Ginolhac],

Sparsity and high dimension: [A. Bitar, J.P. Ovarlez].

Acknowledgements

- Frédéric Pascal, LSS CentraleSupelec, Gif sur Yvette, France,
- Philippe Forster, ENS Cachan, France,
- Guillaume Ginolhac, Annecy University, France,
- and former PhD Students: M. Mahot, P. Formont, J. Frontera-Pons, A. Breloy, ...

References

Many references relative to this seminar can be found on my homepage:

<http://www.jeanphilippeovarlez.com>

References I



Bertrand, J. and Bertrand, P. (1996).

The concept of hyperimage in wide-band radar imaging.

Geoscience and Remote Sensing, IEEE Transactions on, 34(5):1144–1150.



Bertrand, J., Bertrand, P., and Ovarlez, J. P. (1991).

Dimensionalized wavelet transform with application to radar imaging.

In *Proc. IEEE International Conference on Acoustics, Speech, and Signal Processing (ICASSP'91)*, volume 4, pages 2909–2912, Toronto, Canada.



Bertrand, J., Bertrand, P., and Ovarlez, J. P. (1994).

Frequency directivity scanning in laboratory radar imaging.

International Journal of Imaging Systems and Technology, 5(1):39–51.



Conte, E., Lops, M., and Ricci, G. (1995).

Asymptotically optimum radar detection in compound-gaussian clutter.

Aerospace and Electronic Systems, IEEE Transactions on, 31(2):617–625.



Frontera-Pons, J., Pascal, F., and Ovarlez, J. P. (2017).

Adaptive nonzero-mean gaussian detection.

Geoscience and Remote Sensing, IEEE Transactions on, 55(2):1117–1124.



Frontera-Pons, J., Veganzones, M. A., Pascal, F., and Ovarlez, J. P. (2016).

Hyperspectral anomaly detectors using robust estimators.

IEEE Journal of Selected Topics in Applied Earth Observations and Remote Sensing, 9(2):720–731.

References II



Frontera-Pons, J., Veganzones, M. A., Velasco-Forero, S., Pascal, F., Ovarlez, J. P., and Chanussot, J. (2014). Robust anomaly detection in hyperspectral imaging.
In 2014 IEEE Geoscience and Remote Sensing Symposium, pages 4604–4607.



Ginolhac, G., Forster, P., Ovarlez, J.-P., and Pascal, F. (2011). STAP à Rand Réduit, Robuste et Persymétrique.
Traitements du Signal, 28(1-2):143–170.
Numéro Spécial : Traitements Spatio-Temporels Adaptatifs (STAP).



Ginolhac, G., Forster, P., Pascal, F., and Ovarlez, J. P. (2012). Derivation of the bias of the normalized sample covariance matrix in a heterogeneous noise with application to low rank STAP filter.
Signal Processing, IEEE Transactions on, 60(1):514–518.



Ginolhac, G., Forster, P., Pascal, F., and Ovarlez, J. P. (2013). Performance of two low-rank STAP filters in a heterogeneous noise.
Signal Processing, IEEE Transactions on, 61(1):57–61.



Greco, M. S. and Maio, A. D., editors (2016). *Modern Radar Detection Theory*. SciTech Publishing.



Kraut, S. and Scharf, L. (1999). The CFAR adaptive subspace detector is a scale-invariant GLRT.
Signal Processing, IEEE Transactions on, 47(9):2538–2541.

References III



Mian, A., Ovarlez, J. P., Ginolhac, G., and Atto, A. M. (2017).

Multivariate change detection on high resolution monovariate SAR image using linear time-frequency analysis.
In Proc. EURASIP XXV European Signal Processing Conference (EUSIPCO'17), Kos Island, Greece.



Ovarlez, J., Pang, S., Pascal, F., Achard, V., and Ng, T. (2011a).

Robust detection using the SIRV background modelling for hyperspectral imaging.
In Geoscience and Remote Sensing Symposium (IGARSS), 2011 IEEE International, pages 4316–4319.



Ovarlez, J. P., Ginolhac, G., and Atto, A. M. (2017).

Multivariate linear time-frequency modeling and adaptive robust target detection in highly textured monovariate SAR image.

In 2017 IEEE International Conference on Acoustics, Speech and Signal Processing (ICASSP), pages 4029–4033.



Ovarlez, J.-P., Pascal, F., Forster, P., Ginolhac, G., and Mahot, M. (2011b).

Traitements STAP et Modélisation SIRV : Robustesse et Persymétrie.

Traitements du Signal, 28(1-2):113–142.

Numéro Spécial : Traitements Spatio-Temporels Adaptatifs (STAP).



Pailloux, G. (2010).

Estimation Structurée de la Matrice de Covariance et Application à la Détection Radar.

PhD thesis, University of Nanterre / ONERA, France.



Pailloux, G., Forster, P., Ovarlez, J.-P., and Pascal, F. (2011).

Persymmetric adaptive radar detectors.

Aerospace and Electronic Systems, IEEE Transactions on, 47(4):2376–2390.

References IV

-  Pascal, F. (2006).
Détection et Estimation en Environnement Non-Gaussien.
PhD thesis, University of Nanterre / ONERA, France.
-  Pascal, F., Chitour, Y., Ovarlez, J. P., Forster, P., and Larzabal, P. (2008).
Covariance structure maximum-likelihood estimates in compound gaussian noise: Existence and algorithm analysis.
Signal Processing, IEEE Transactions on, 56(1):34–48.
-  Pascal, F., Chitour, Y., and Quek, Y. (2014).
Generalized robust shrinkage estimator and its application to STAP detection problem.
Signal Processing, IEEE Transactions on, 62(21):5640–5651.
-  Pascal, F., Ovarlez, J.-P., Forster, P., and Larzabal, P. (2006).
On a SIRV-CFAR detector with radar experimentations in impulsive noise.
In *Proc. of the European Signal Processing Conf.*, Florence.
-  Reed, I. and Yu, X. (1990).
Adaptive multiple-band CFAR detection of an optical pattern with unknown spectral distribution.
Acoustics, Speech and Signal Processing, IEEE Transactions on, 38(10):1760–1770.